

# Supplementary Figures

## Alkaline phosphatase controls lineage switching of mesenchymal stem cells by regulating the LRP6/GSK3 $\beta$ complex in hypophosphatasia

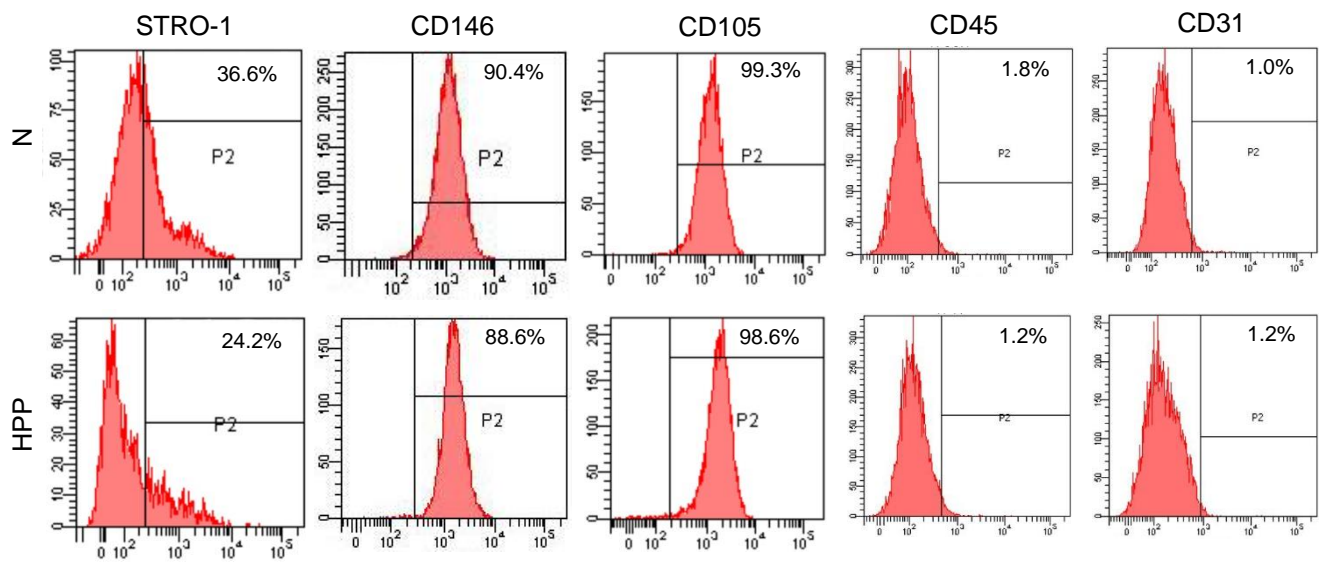
Wenjia Liu<sup>1,2,#</sup>, Liqiang Zhang<sup>1,2,#</sup>, Kun Xuan<sup>1,#</sup>, Chenghu Hu<sup>2</sup>, Liya Li<sup>2</sup>, Yongjie Zhang<sup>2</sup>, Fang Jin<sup>1\*</sup>, Yan Jin<sup>1,2,\*</sup>

1. MS-State Key Laboratory & National Clinical Research Center for Oral Diseases & Shaanxi International Joint Research Center for Oral Diseases, Center for Tissue Engineering, School of Stomatology, Fourth Military Medical University, Xi'an, 710032, China.

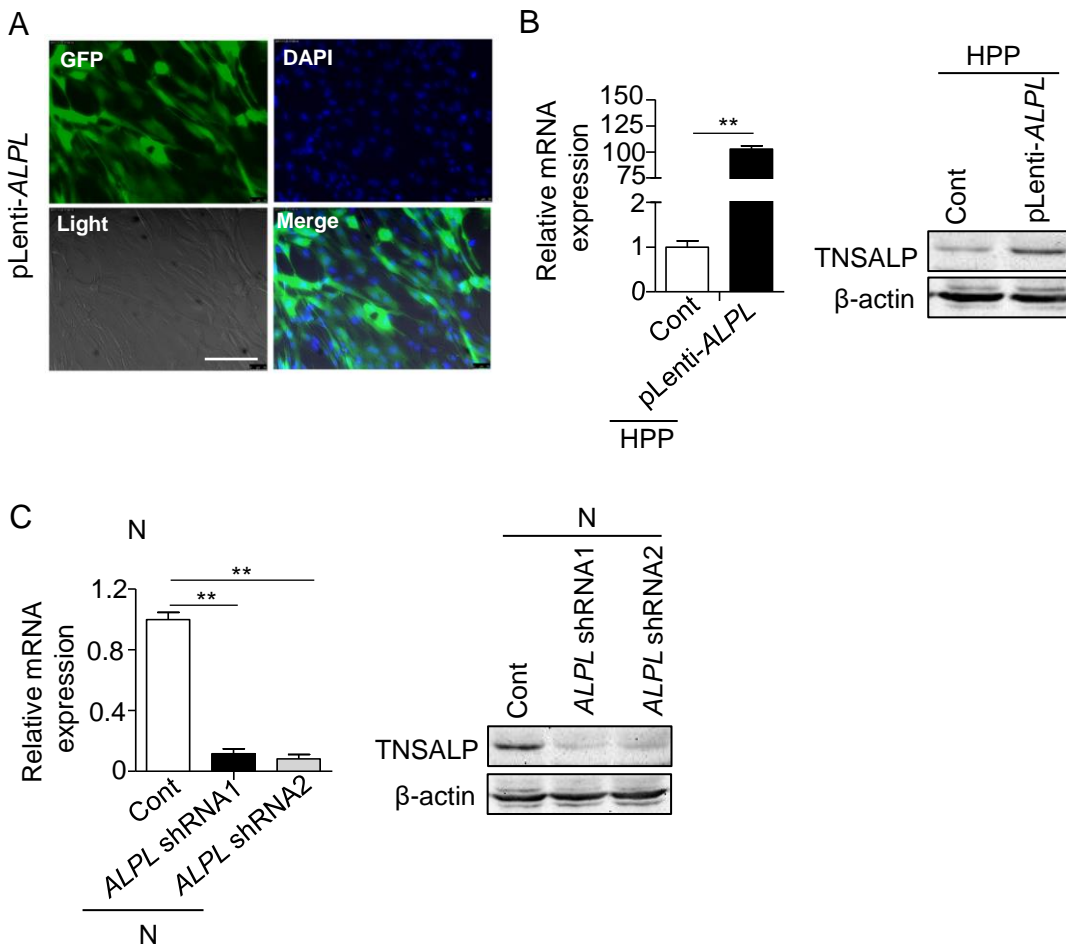
2. Xi'an Institute of Tissue Engineering and Regenerative Medicine, Xi'an, 710032, China.

# W.J.L, L.Q.Z and K.X. made equal contribution.

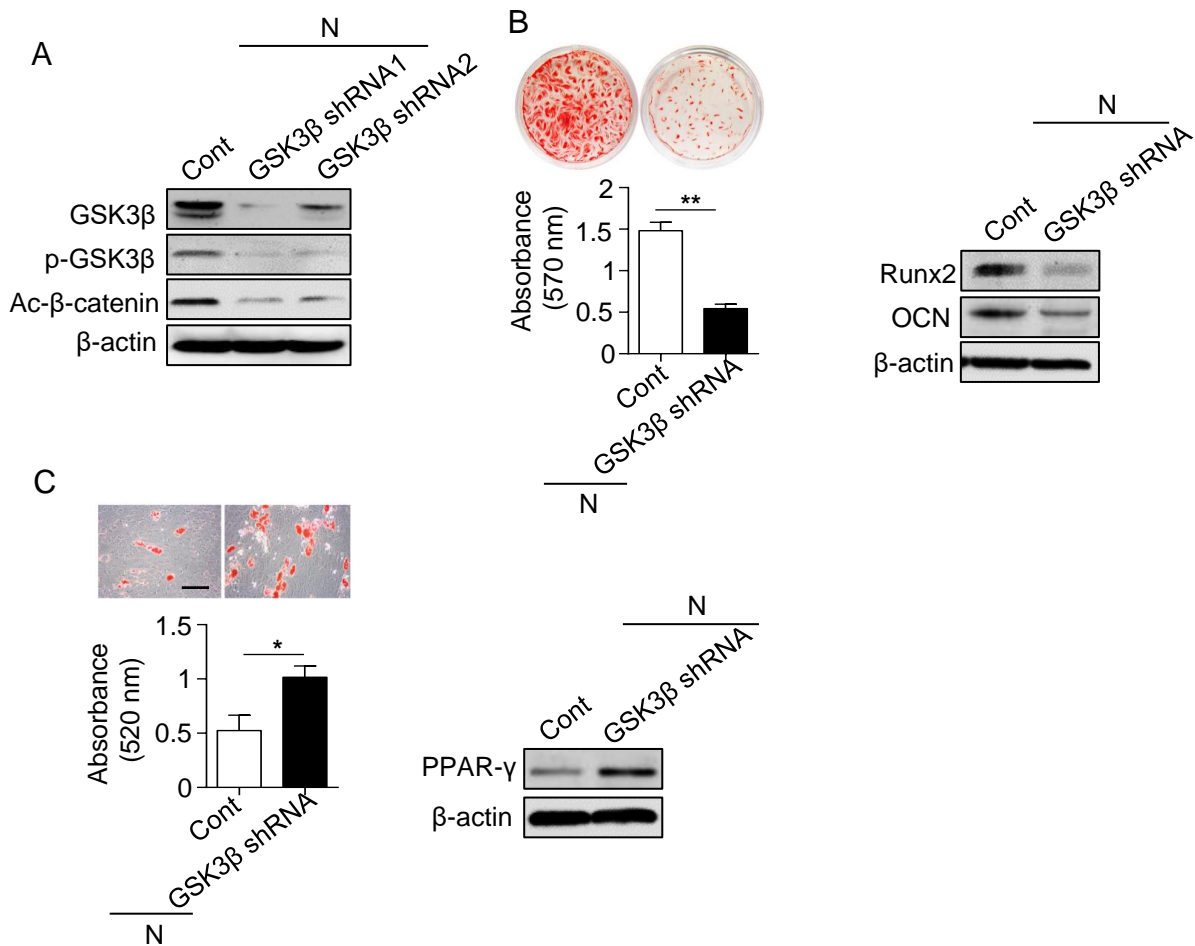
\*Corresponding authors: Yan Jin, School of Stomatology, Fourth Military Medical University, 145 West Chang Le Road, Xin cheng District, Xi'an, China, 710032; e-mail: yanjin@fmmu.edu.cn; Fang Jin, School of Stomatology, Fourth Military Medical University, 145 West Chang Le Road, Xin cheng District, Xi'an, China, 710032; e-mail: jinfang@fmmu.edu.cn.



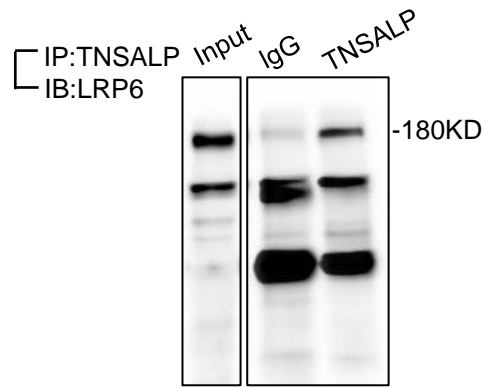
**Supplementary Figure 1. The identification of human BMMSCs, related to Figure 2.** The surface markers of BMMSCs, including STRO-1, CD146, CD105, CD45 and CD31 were analyzed by flow cytometry. Normal control n = 5, HPP n = 2.



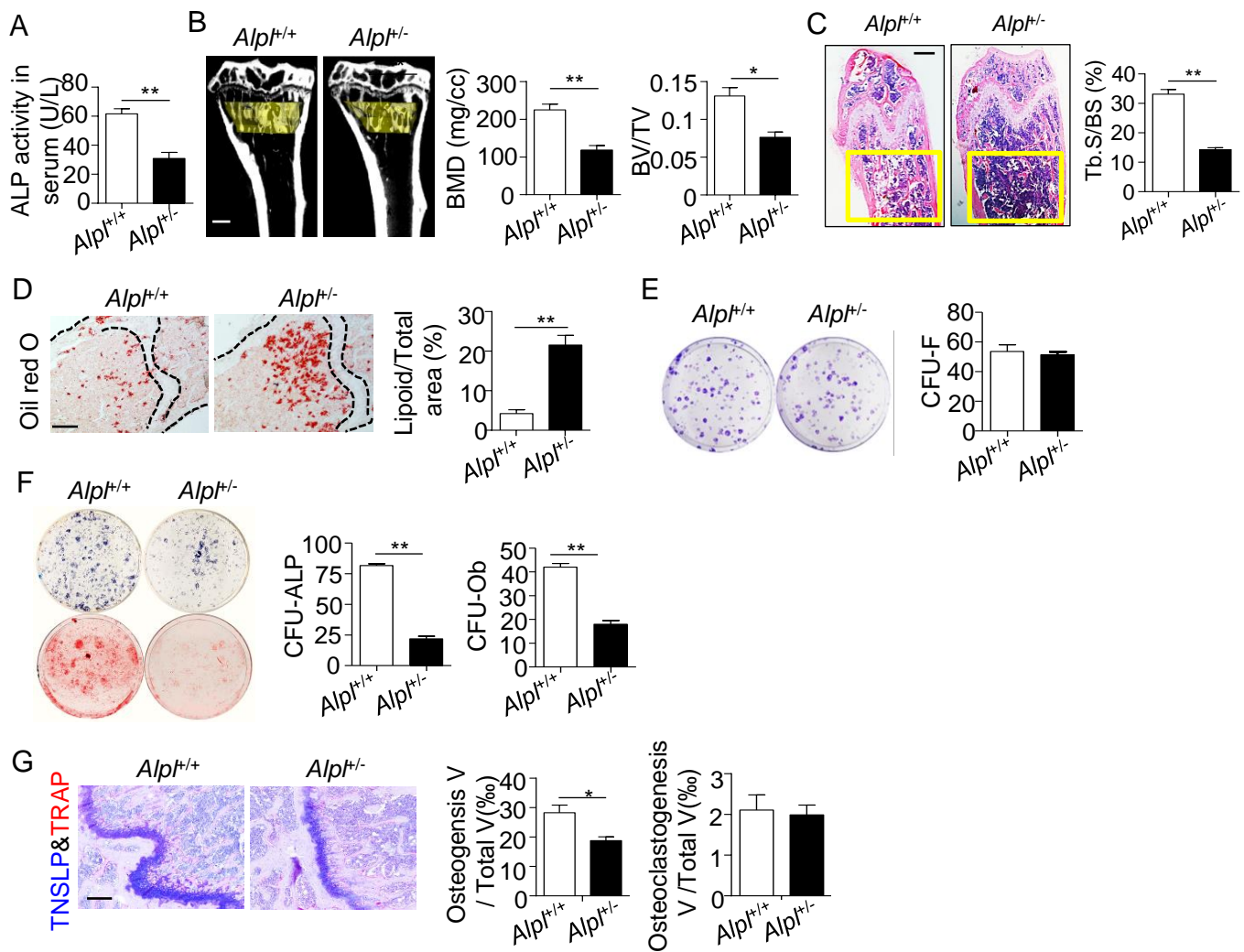
**Supplementary Figure 2. The efficiency of lentiviral vector transduction, related to Figure 3. (A)** Effect of lentiviral vector transduction for upregulating *ALPL* was shown by laser confocal microscopy analyses. Scale bars, 100  $\mu$ m. **(B, C)** Efficiency of lentiviral vector on knockdown or overexpressing *ALPL* was confirmed by qRT-PCR and western blotting. Normal control n = 5, HPP n = 2. The data are presented as means  $\pm$  s.d. for triplicate samples from a representative experiment. \* $P$  < 0.05, \*\* $P$  < 0.01. B, Unpaired two-tailed Student's t-test. C, One-way analysis of variance (ANOVA).



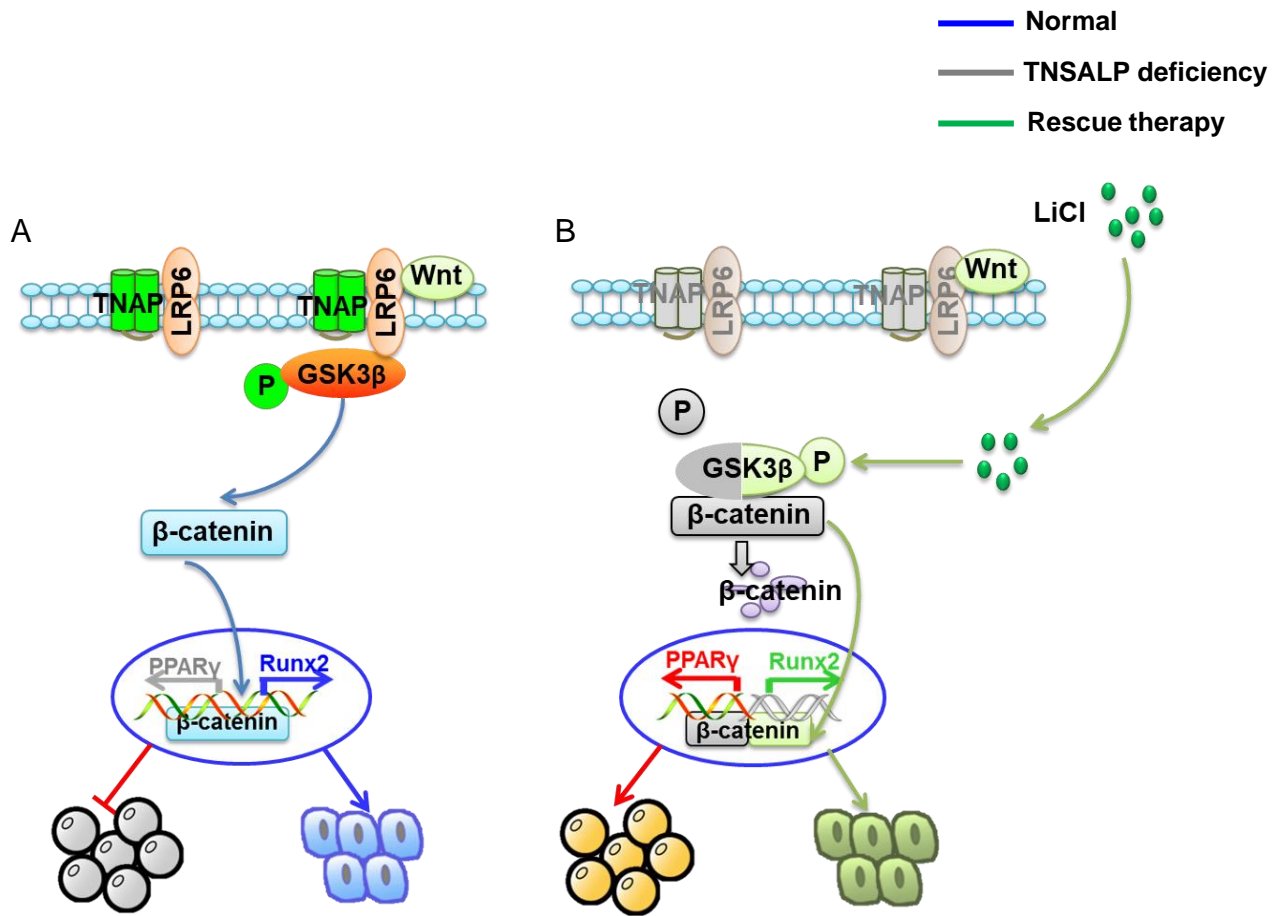
**Supplementary Figure 3. Downregulation of GSK3β inhibits osteogenic differentiation but promotes adipogenic differentiation of BMMSCs, related to Figure 4. (A)** Western blotting of total GSK3β and p-GSK3β in normal BMMSCs transduced with GSK3β downregulation lentivirus. **(B)** Alizarin red staining and quantification of mineralized nodules were performed at day 28 after osteogenic induction in normal control and GSK3β shRNA transduction group. Expression levels of Runx2 and OCN were examined at day 7 after induction by western blotting. **(C)** Oil Red O staining and quantification of fat depots were performed at day 14 after adipogenic induction. PPAR-γ expression was examined at day 7 after induction by western blotting.  $n = 5$  for all group. Scale bars, 100 μm. The data are presented as means  $\pm$  s.d. for triplicate samples from a representative experiment.  $*P < 0.05$ ,  $**P < 0.01$ . Unpaired two-tailed Student's t-test.



**Supplementary Figure 4. Direct binding of TNSALP and LRP6 was confirmed in WT BMMSCs, related to Figure 5.** TNSALP immunoprecipitated LRP6. Left panel showed the expression of LRP6, and right panel showed the level of LRP6 following immunoprecipitation with an anti-TNSALP antibody. n = 6 per group.



**Supplementary Figure 5. Heterozygous *Alpl*<sup>+/-</sup> mice exhibit a decrease in bone mass and a parallel increase of bone marrow fat, related to Figure 7. (A)** Serum ALP activity in 4 month wild-type (WT) and *Alpl*<sup>+/-</sup> mice. **(B)** Representative  $\mu$ CT images of tibia. Quantitative  $\mu$ CT analysis of BMD and BV/TV in WT and *Alpl*<sup>+/-</sup> mice tibia. Scale bars, 1 mm. **(C)** Femur trabecular bone volume was evaluated by hematoxylin and eosin staining (H&E) analysis. Scale bars, 1 mm. **(D)** Representative Oil Red O staining images and quantitative analysis of the area of adipose tissue over the total area of the proximal femoral diaphysis. Scale bars, 500  $\mu$ m. **(E, F)** CFU-F, CFU-ALP (top panels) and CFU-Ob (bottom panels) assays from harvested BMMSCs and quantitative analyses were indicated in right panel. **(G)** TNSALP&TRAP staining showed osteogenesis and osteoclastogenesis in both WT and *Alpl*<sup>+/-</sup> mice. Quantifications were indicated at bottom panel. n = 6 per group. Scale bars, 200  $\mu$ m. Data shown as mean  $\pm$  s.d. \**P* < 0.05, \*\**P* < 0.01. Unpaired two-tailed Student's t-test. *Alpl*<sup>+/+</sup>: wild-type littermates. *Alpl*<sup>+/-</sup>: heterozygous *Alpl* knockout mice.



**Supplementary Figure 6. Schematic diagram depicting how TNSALP controls lineage switching of BMMSCs by regulating the LRP6/GSK3 $\beta$  cascade and therapeutic methods. (A)** Physiologically, TNSALP interacted with LRP6 leads to the phosphorylation of GSK3 $\beta$  and lets  $\beta$ -catenin get into nucleus. This action subsequently activates canonical Wnt pathway and promotes osteogenesis (Runx2). **(B)** When TNSALP deficiency, Wnt signal could not phosphorylate GSK3 $\beta$  and prevents  $\beta$ -catenin getting into nucleus, which then inactivates canonical Wnt pathway and inhibits osteogenesis but enhances adipogenesis (PPAR $\gamma$ ). Small molecular LiCl rephosphorylated GSK3 $\beta$ , which facilitates the movement of  $\beta$ -catenin into nucleus to rescue the lineage differentiation of BMMSCs and alleviates skeletal deformities in *Alpl*<sup>+/-</sup> mice.